Published October 4, 2010





# The differential interaction of snRNPs with pre-mRNA reveals splicing kinetics in living cells

Martina Huranová,[1] Ivan Ivani,[1] Aleš Benda,[2] Ina Poser,[3] Yehuda Brody,[4,5] Martin Hof,[2] Yaron Shav-Tal,[4,5] Karla M. Neugebauer,[3] and David Staněk[1]

[1]Institute of Molecular Genetics and [2]J. Heyrovský Institute of Physical Chemistry, Academy of Sciences of the Czech Republic, 142 20 Prague, Czech Republic
[3]Max Planck Institute for Molecular Cell Biology and Genetics, 01307 Dresden, Germany
[4]The Mina and Everard Goodman Faculty of Life Sciences and [5]Institute for Nanotechnology and Advanced Materials, Bar-Ilan University, Ramat Gan 52900, Israel

Precursor messenger RNA (pre-mRNA) splicing is catalyzed by the spliceosome, a large ribonucleoprotein (RNP) complex composed of five small nuclear RNP particles (snRNPs) and additional proteins. Using live cell imaging of GFP-tagged snRNP components expressed at endogenous levels, we examined how the spliceosome assembles in vivo. A comprehensive analysis of snRNP dynamics in the cell nucleus enabled us to determine snRNP diffusion throughout the nucleoplasm as well as the interaction rates of individual snRNPs with pre-mRNA. Core components of the spliceosome, U2 and U5 snRNPs, associated with pre-mRNA for 15–30 s, indicating that splicing is accomplished within this time period. Additionally, binding of U1 and U4/U6 snRNPs with pre-mRNA occurred within seconds, indicating that the interaction of individual snRNPs with pre-mRNA is distinct. These results are consistent with the predictions of the step-wise model of spliceosome assembly and provide an estimate on the rate of splicing in human cells.

## Introduction

In eukaryotic cells, protein-encoding transcripts contain intronic sequences that must be spliced out before translation. This crucial step in gene expression is catalyzed by the spliceosome, a multicomponent RNP complex which consists of five major U1, U2, U4, U5, and U6 small nuclear RNP particles (snRNPs) in addition to other proteins (for reviews see Will and Lührmann, 2001; Jurica and Moore, 2003; Wahl et al., 2009). Each snRNP consists of a unique small nuclear RNA (snRNA) associated with a specific set of proteins and a ring of seven Sm or Lsm proteins (Urlaub et al., 2001). During splicing, the spliceosome has to accomplish several functions that involve correct intron recognition, a two-step transesterification reaction to cleave out introns and join together exons, and finally the release of mature mRNA (for reviews see Staley and Guthrie, 1998; Wahl et al., 2009).

Although the process of spliceosome assembly has been intensively studied, the precise mechanism of its in vivo formation is still not fully understood. Two models of spliceosome assembly during precursor mRNA (pre-mRNA) splicing have been proposed: (1) the step-wise assembly model, which proposes sequential assembly of individual snRNPs on pre-mRNA, and (2) the penta-snRNP or supraspliceosome model, which predicts that a preformed spliceosome containing all snRNPs is recruited to pre-mRNA (for review see Rino and Carmo-Fonseca, 2009).

According to the step-wise model, snRNPs sequentially interact with the pre-mRNA transcript. Initially, intron boundaries are recognized when the U1 snRNP interacts with the 5′ splice site, and the U2 snRNP and associated factors interact with the branch point. Once the intron is defined, U4, U5, and U6 snRNPs are recruited as a preassembled U4/U6•U5 tri-snRNP. The spliceosome then undergoes extensive conformational and compositional rearrangements that result in the release of U1 and U4 snRNA, together with their corresponding U1 and U4/U6 snRNP–specific proteins, and the formation of the catalytic core that is essential for the transesterification reactions. When splicing is accomplished, mature mRNA is released, and the U2, U5, and U6 snRNPs dissociate from the intron lariat to be recycled for subsequent rounds of splicing. This model is based on numerous

Correspondence to David Staněk: stanek@img.cas.cz

Abbreviations used in this paper: BAC, bacterial artificial chromosome; ChIP, chromatin immunoprecipitation; DRB, 5,6-dichlorobenzimidazole riboside; FCS, fluorescence correlation spectroscopy; pre-mRNA, precursor mRNA; snRNA, small nuclear RNA; snRNP, small nuclear RNP particle.



Supplemental Material can be found at:
http://jcb.rupress.org/content/suppl/2010/09/30/jcb.201004030.DC1.html
Original image data can be found at:
http://jcb-dataviewer.rupress.org/jcb/browse/3011

The Rockefeller University Press $30.00
J. Cell Biol. Vol. 191 No. 1 75–86
www.jcb.org/cgi/doi/10.1083/jcb.201004030

Published October 4, 2010

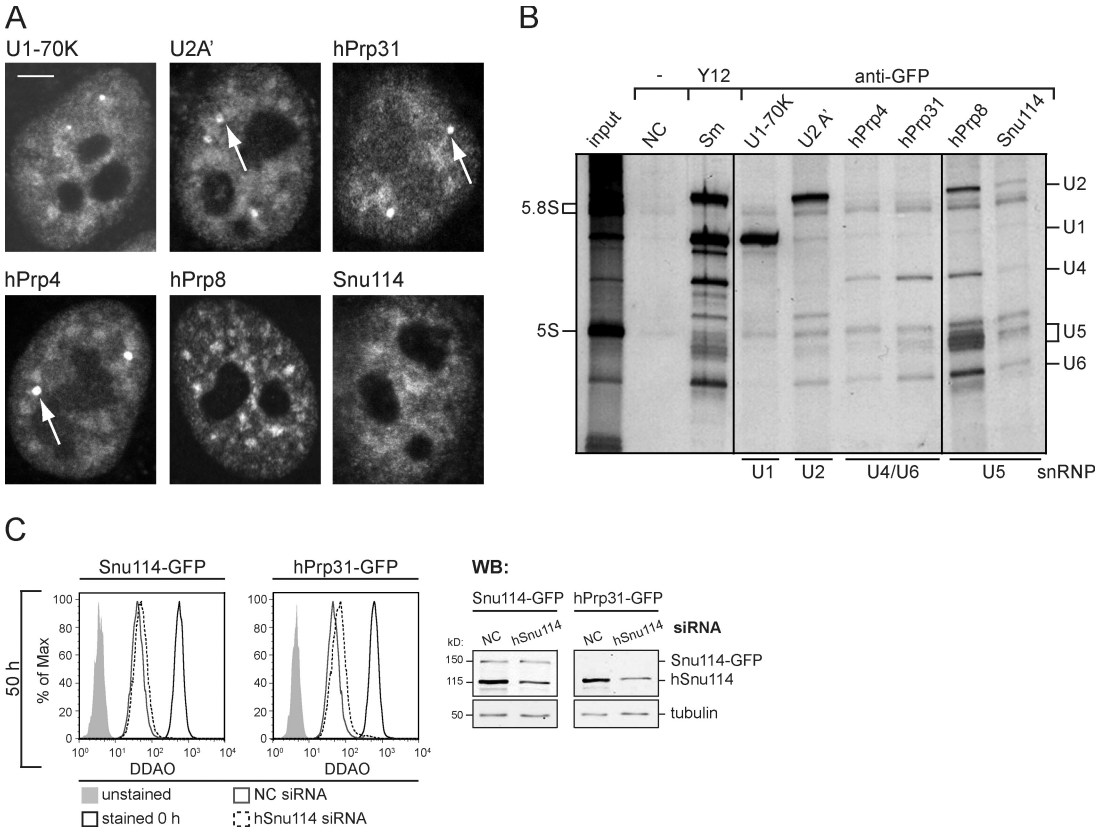


Figure 1. **GFP-tagged snRNP proteins incorporate into snRNPs.** (A) Images of cells expressing GFP-tagged snRNP proteins. GFP-tagged proteins were localized to the nucleoplasm and enriched in splicing factor compartments and Cajal bodies (arrows). Bar, 5 µm. (B) snRNPs were immunoprecipitated using anti-GFP or anti-Sm antibodies, and coprecipitated RNAs were visualized. The positions of snRNAs and rRNAs are depicted. Note that a small amount of U6 and U5 snRNAs coprecipitate with U2 snRNP (U2A′ line) and U2 snRNA associated with U5 snRNP (hPrp8 and Snu114 lines). Vertical black lines indicate that intervening lanes have been spliced out. (C) Proliferation of control cells (hPrp31-GFP) and cells expressing mouse Snu114-GFP was assayed by DDAO staining after knockdown of endogenous hSnu114. Reduction of hSnu114 levels (see Western blot [WB]) resulted in proliferation defects that were partially rescued by expression of RNAi-resistant mouse Snu114-GFP. NC, negative control.

in vitro observations that demonstrated the sequential association of individual snRNPs with pre-mRNA (Reed, 2000). Furthermore, in both yeast and mammalian in vitro systems, distinct intermediates of spliceosome assembly were detected and characterized (Brody and Abelson, 1985; Konarska and Sharp, 1986; Bindereif and Green, 1987; Jurica et al., 2002; for review see Jurica and Moore, 2003). Finally, in yeast cells, chromatin immunoprecipitation (ChIP) data showed the sequential association of snRNPs with nascent transcripts (Kotovic et al., 2003; Görnemann et al., 2005; Lacadie and Rosbash, 2005; Tardiff and Rosbash, 2006; Tardiff et al., 2006). However, in mammalian cells, ChIP lacks the necessary resolution to analyze the dynamic aspects of spliceosome assembly (Listerman et al., 2006).

The second model proposes the existence of a preassembled spliceosome that is splicing competent. Multiple studies performed in yeast and mammalian systems have demonstrated the association of U1 and U2 snRNPs with U4/U6 and U4/U6•U5 snRNPs in the absence of pre-mRNA (Konarska and Sharp, 1988; Wassarman and Steitz, 1992). This alternative view was supported when the 45S complex was isolated from a yeast extract and was found to contain all five snRNPs. Subsequently, this complex was referred to as the penta-snRNP (Stevens et al., 2002). Additionally, in human cells, a large 200S RNP particle named the supraspliceosome that contained four penta-snRNP–like subunits was isolated and shown to catalyze RNA splicing (Azubel et al., 2006; Sperling et al., 2008). However, it was also reported in a human in vitro system that the penta-snRNP is not essential for early spliceosome assembly steps (Behzadnia et al., 2006). Fluorescence resonance energy transfer studies performed in live cells showed that the interaction between several splicing factors persisted after transcriptional inhibition, indicating that the larger splicing complexes are formed in vivo in the absence of pre-mRNA (Chusainow et al., 2005; Ellis et al., 2008; Rino et al., 2008).

To elucidate the dynamic properties of snRNPs and their interactions with pre-mRNA in vivo, we used fluorescence correlation spectroscopy (FCS) and FRAP. Live cell imaging techniques have previously been used to investigate the dynamic properties of several macromolecular complexes, including splicing factors and RNA polymerases (Dundr et al., 2002; Darzacq et al., 2007; Rino et al., 2007; Gorski et al., 2008) as well as the assembly of the exon junction complex (Schmidt et al., 2009). We took advantage of stable cell lines that contained integrated bacterial artificial chromosomes (BACs) that encoded recombinant GFP-tagged snRNP proteins expressed under endogenous regulatory elements. Thus, the expression of GFP-tagged snRNP proteins mimics the expression of their endogenous counterparts (Poser et al., 2008; Sapra et al., 2009). Analysis of the dynamic behavior of snRNP-specific proteins in the cell nucleus revealed

Published October 4, 2010

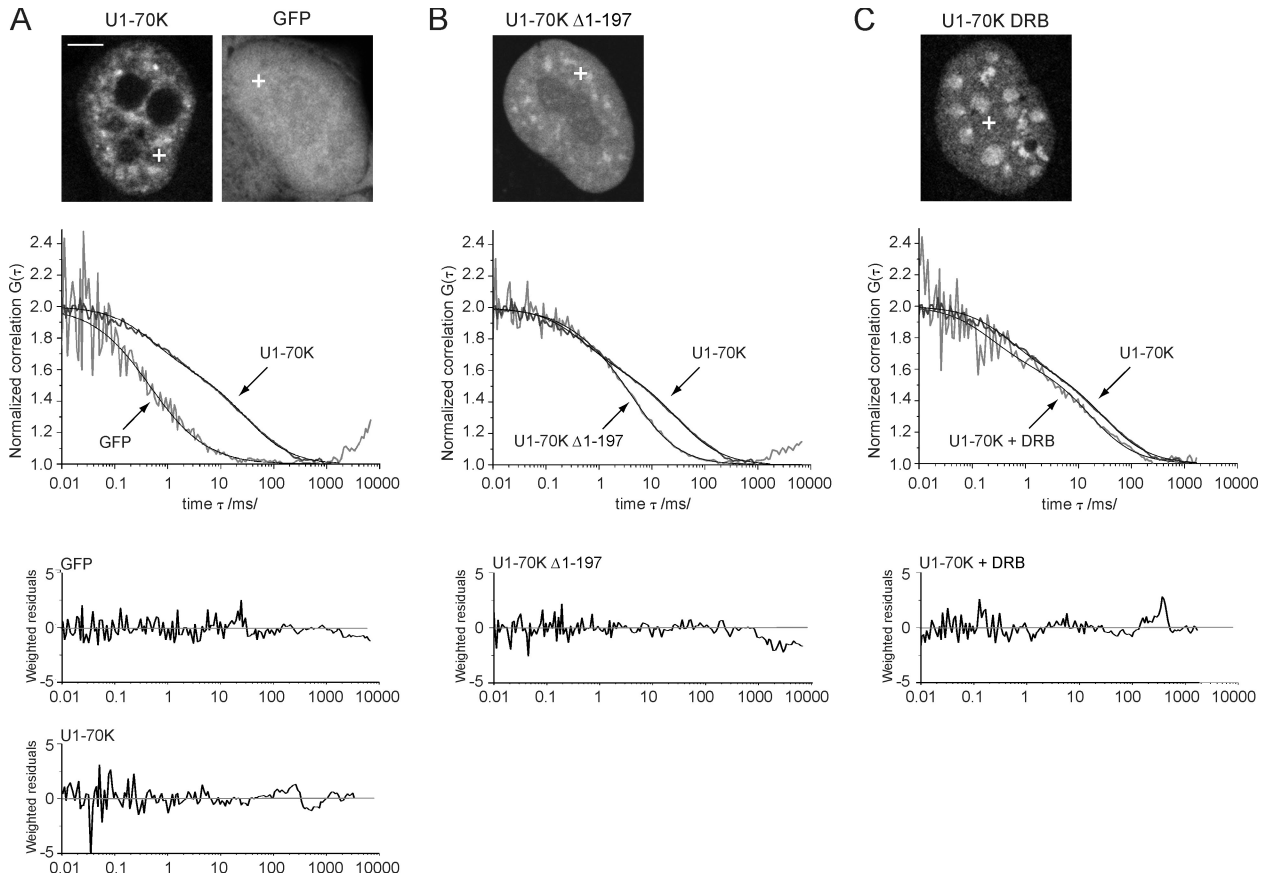


Figure 2. **FCS measures the in vivo mobility of snRNPs.** (A) FCS measurements were performed in the nucleoplasm of cells either stably expressing U1-70K–GFP or transiently expressing GFP. The autocorrelation function of free GFP is fitted with a one-component anomalous diffusion model. The autocorrelation function of U1-70K is fitted with a two-component diffusion model. (B) The autocorrelation function of U1-70KΔ1–197 is fitted with a two-component diffusion model. Deletion of the RNA-binding domain of U1-70K results in a fourfold increase in diffusion of the slow component. (C) DRB treatment (5 h) inhibits RNA polymerase II and results in the enlargement and rounding up of splicing factor compartments. DRB treatment had only a minimal effect on snRNP diffusion, with both fast and slow components still present. (A–C) Crosses indicate spots in the nucleoplasm where FCS measurements were performed, and weighted residuals are shown to assess the fit quality. Bar, 5 µm.

the intricate details of spliceosomal complex formation. In addition, we were able to estimate the rate of splicing in living human cells by analyzing the interaction between the core spliceosomal snRNPs with pre-mRNA.

## Results

### FCS reveals the diffusion properties of the snRNP mobile fraction

To describe the dynamic behavior of snRNPs in living cells, we established stable HeLa cell lines that express from BACs the GFP-tagged snRNP proteins U2A′ (U2 snRNP), hPrp31 and hPrp4 (U4/U6 snRNP), and Snu114 (U5 snRNP). Previously used HeLa cell lines expressing BAC-encoded GFP-tagged snRNP proteins, U1-70K (U1 snRNP) and hPrp8 (U5 snRNP), were also used (Sapra et al., 2009). The advantage of using BACs for gene expression experiments is that the endogenous regulatory elements are preserved, allowing their expression to be similar to that of the endogenous protein. The expression of GFP-tagged snRNP proteins did not impair cotranscriptional spliceosome formation, and haploid yeast cells that express only GFP-tagged snRNP proteins remained viable without any defects in pre-mRNA splicing (Görnemann et al., 2005; Sapra et al., 2009). GFP-tagged snRNP proteins were properly localized to the cell nucleus and accumulated in Cajal bodies (Fig. 1 A). Immunoprecipitation followed by snRNA analysis revealed that the GFP-tagged proteins were properly incorporated into the appropriate snRNPs (Fig. 1 B). In addition, knockdown of endogenous Snu114 by RNAi reduced the proliferation rate of control hPrp31-GFP by 20% in comparison with cells expressing RNAi-resistant mouse Snu114-GFP (Fig. 1 C). We concluded that the GFP-tagged snRNP proteins behaved analogously to their endogenous counterparts and were suitable for further investigation.

To analyze the movement of snRNPs in the cell nucleus, we first used FCS, a tool sensitive enough to detect rapid diffusion and fast interactions (Kim et al., 2007). This technique focuses a laser beam on a spot of interest in the nucleoplasm and monitors fluctuations in fluorescence intensity over time. The intensity record is transformed into an autocorrelation function that assesses the diffusion correlation time of the detected molecules. FCS measurements were performed within the nucleoplasm and compared with the splicing factor compartments (also termed nuclear speckles; Fig. 2 A and Table I; Neugebauer, 2002; Lamond and Spector, 2003). By using the pure diffusion model (Eq. 1),

Published October 4, 2010

Table I. **Calculated parameters derived from FCS measurements**

| Proteins | Nucleoplasm | | | | Splicing factor compartments | | | |
|---|---|---|---|---|---|---|---|---|
| | $\tau_{Da}$ | $D_{fa}$ | $\tau_{Db}$ | $D_{fb}$ | $\tau_{Da}$ | $D_{fa}$ | $\tau_{Db}$ | $D_{fb}$ |
| | *ms* | $\mu m^2 s^{-1}$ | *ms* | $\mu m^2 s^{-1}$ | *ms* | $\mu m^2 s^{-1}$ | *ms* | $\mu m^2 s^{-1}$ |
| U1-70K[a] | 0.56 ± 0.08 | 28.21 ± 4.22 | 24.92 ± 3.08 | 0.63 ± 0.08 | 0.67 ± 0.17 | 24.98 ± 7.41 | 33.68 ± 3.77 | 0.47 ± 0.05 |
| U2A′[a] | 0.67 ± 0.18 | 24.85 ± 6.87 | 19.91 ± 4.68 | 0.82 ± 0.20 | 0.72 ± 0.11 | 22.30 ± 3.70 | 26.82 ± 5.98 | 0.61 ± 0.15 |
| hPrp31[a] | 0.99 ± 0.23 | 16.74 ± 5.40 | 18.08 ± 3.13 | 0.88 ± 0.15 | 0.97 ± 0.12 | 16.27 ± 2.01 | 20.55 ± 4.49 | 0.79 ± 0.18 |
| hPrp4[a] | 0.76 ± 0.17 | 21.35 ± 4.49 | 24.68 ± 3.03 | 0.64 ± 0.08 | 1.06 ± 0.35 | 15.96 ± 4.54 | 22.46 ± 2.83 | 0.71 ± 0.10 |
| hPrp8[a] | 0.64 ± 0.12 | 24.97 ± 4.50 | 30.29 ± 1.44 | 0.52 ± 0.02 | 0.78 ± 0.16 | 20.79 ± 4.34 | 33.83 ± 4.91 | 0.47 ± 0.07 |
| Snu114[a] | 0.76 ± 0.24 | 22.09 ± 5.83 | 26.45 ± 5.16 | 0.61 ± 0.12 | 1.01 ± 0.09 | 15.58 ± 1.47 | 27.18 ± 2.78 | 0.58 ± 0.06 |
| U1-70KΔ1–197 | 0.58 ± 0.19 | 28.81 ± 6.36 | 6.80 ± 1.50 | 2.40 ± 0.55 | 0.82 ± 0.10 | 19.39 ± 6.36 | 6.18 ± 1.89 | 2.70 ± 0.66 |
| EGFP | 0.56 ± 0.05 | 27.87 ± 2.22 | NA | NA | ND | ND | ND | ND |

NA, not applicable. Dynamics of snRNP proteins were measured in the nucleoplasm and the splicing factor compartments by FCS. The delay time values $\tau_{Da}$ for EGFP are comparable with the values of the fast component detected in the FCS measurements of snRNP proteins. The values for the delay times $\tau_{Db}$ describe the diffusion of the slow-moving component that reflects snRNP complexes. $\tau_{Da}$ and $\tau_{Db}$ were used to calculate the diffusion coefficients $D_{fa}$ and $D_{fb}$, respectively. The mean ± SD from 8–10 cells is shown.

[a]BAC stable cell line.

a satisfactory fit of autocorrelation function was achieved (Kim et al., 2007). We detected two moving components in the nucleoplasm of each cell line expressing GFP-tagged snRNP proteins, with diffusion correlation times of around 1 ms for the fast component ($\tau_{Da}$, ∼40% of all moving proteins) and 20–30 ms for the slow component ($\tau_{Db}$, ∼60% of all moving proteins; Fig. 2 A and Table I). Two populations were detected in the splicing factor compartments as well, and both components exhibited reduced diffusion in contrast to the nucleoplasm (Table I).

The correlation times of the fast component were similar to free GFP and likely reflected free proteins (Fig. 2 A and Table I). To elucidate whether the slow component represented snRNP complexes, we constructed a truncated form of the U1-70K protein lacking the first 1–197 aa that contain the U1 snRNA–binding motif (Nelissen et al., 1994). In agreement with previous results that demonstrated that the C-terminal domain is still able to interact with non-snRNP proteins (Cao and Garcia-Blanco, 1998), we observed that the transiently expressed U1-70KΔ1–197–GFP protein partially accumulated in splicing factor compartments (Fig. 2 B) but did not incorporate into the U1 snRNP (Fig. S1 A). FCS measurements revealed that deletion of the RNA-binding motif did not affect diffusion of the fast component but resulted in a dramatic decrease of the delay time of the slow component pointing to approximately fourfold faster movement of complexes containing the truncated protein (Fig. 2 B and Table I). We conclude that FCS measurements of wild-type snRNP proteins reveal the diffusion properties of snRNP complexes.

To examine whether the snRNP movement in the nucleoplasm is affected by its interaction with pre-mRNA, we treated cells with 5,6-dichlorobenzimidazole riboside (DRB), a potent inhibitor of RNA polymerase II (Chodosh et al., 1989). The treatment resulted in an enlargement of splicing factor compartments (Fig. 2 C) and inhibited RNA synthesis (Fig. S2). FCS measurements revealed that transcriptional inhibition had little effect on the diffusional behavior of snRNPs in the nucleoplasm (Fig. 2 C). In summary, using FCS, we showed that individual snRNPs diffused rapidly throughout the nucleoplasm with comparable diffusion correlation times (Table I). However, we were not able to detect any stable interactions between individual snRNPs and pre-mRNA. We predict that these interactions occur over a longer time scale (seconds and more) beyond the detection limit of FCS.

## snRNP diffusion measured by FRAP correlates with FCS data

To overcome the limits of FCS, we used FRAP to elucidate the relatively slow interaction of snRNPs with pre-mRNA. The FRAP method involves photobleaching of a small area within the sample and monitoring the recovery of fluorescence intensity over time. Fluorescence recovery reflects the movement of unbleached molecules into the bleached area and is determined by the diffusion and binding characteristics of the analyzed molecules (Sprague et al., 2004; Sprague and McNally, 2005; McNally, 2008). Importantly, pre-mRNA splicing is largely cotranscriptional (Neugebauer, 2002) and is significantly faster compared with RNA polymerase II elongation (Singh and Padgett, 2009). With respect to mobile snRNPs, pre-mRNA represents an immobilized substrate. To dissect diffusion from binding events, we compared the dynamics of snRNPs in the nucleoplasm before and after transcriptional inhibition (Fig. 3, A–D). FRAP measurements in DRB-treated cells showed fast and full fluorescence recovery (Fig. 3, B–D), indicating that transcriptional inhibition depleted pre-mRNA–binding sites. Recovery curves were fitted with the pure diffusion model (Eq. 2), supporting the assumption that in the absence of pre-mRNA, snRNPs move rapidly throughout the nucleoplasm. Quantification of FRAP curves yielded effective diffusion coefficients ranging from 0.2 to 0.6 $\mu m^2 s^{-1}$ (Table II), which were comparable with the diffusion coefficient range of 0.5–0.9 $\mu m^2 s^{-1}$ obtained by FCS (Table I). As the diffusion coefficients are lower than diffusion coefficients of freely diffusing macromolecular complexes of snRNP size (∼1 MD), these data indicate that in DRB-treated cells, both FRAP and FCS measured the effective diffusion, which is a combination of relatively low affinity binding events and free diffusion.

Increased mobility of snRNPs in the splicing factor compartments after transcriptional inhibition indicated that snRNPs interact with pre-mRNA in these compartments, as suggested previously (Rino et al., 2007). Although DRB treatment resulted in complete fluorescence recovery in the nucleoplasm, we detected ∼10%

Published October 4, 2010

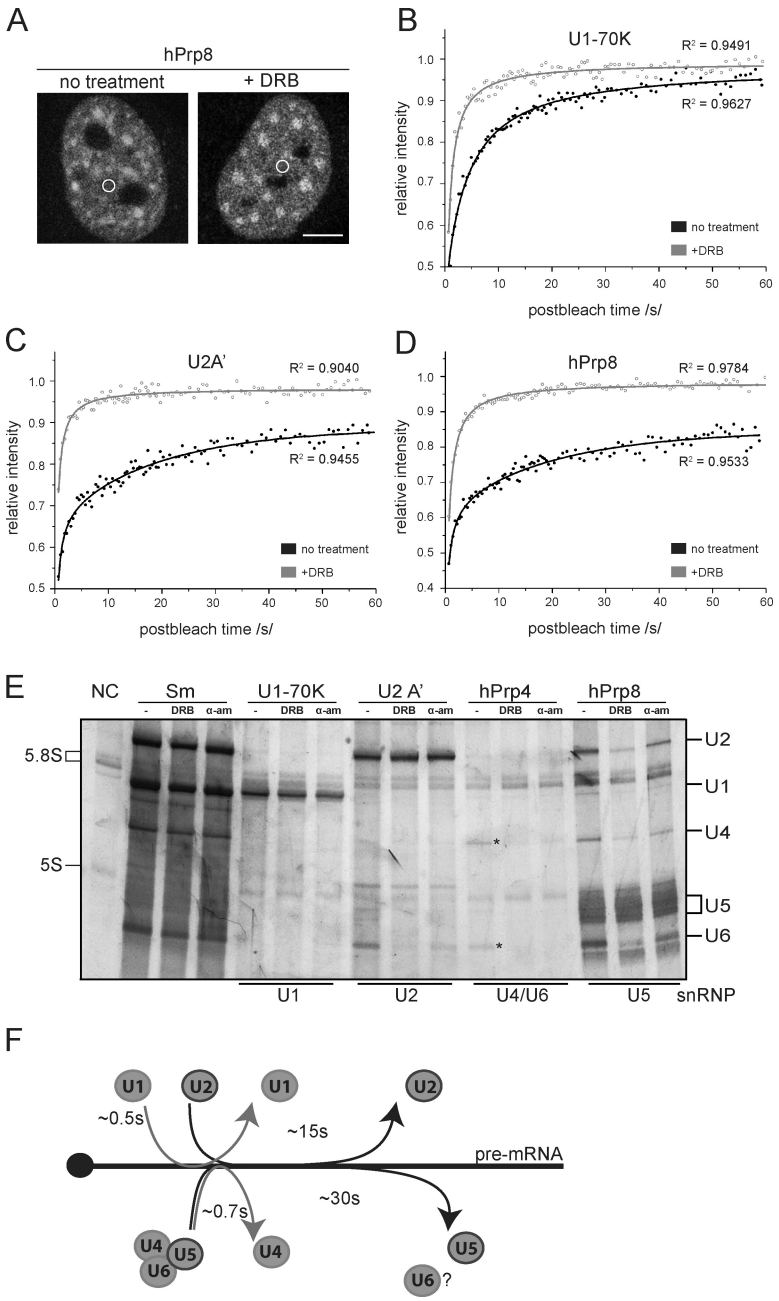


Figure 3. **snRNPs interact independently with pre-mRNA, as analyzed by FRAP.** (A) FRAP measurements were performed in the nucleoplasm, as depicted by circles. Bar, 5 µm. (B–D) U1-70K (B), U2A′ (C), and hPrp8 (D) FRAP curves representing a mean of 10–15 measurements before and after DRB treatment are shown. FRAP curves were fitted either with a pure diffusion model (DRB treatment) or the full model (no treatment). Calculated diffusion coefficients and dissociation constants $k_{off}$ are shown in Table II. $R^2$ values evaluating fit quality are shown next to the curves. (E) Coimmunoprecipitation of snRNAs with anti-GFP antibodies from U1-70K-GFP, U2A′-GFP, hPrp4-GFP, and hPrp8-GFP cell lines before and after DRB or α-amanitin treatment. Transcriptional inhibition had no effect on the precipitation of U1 and U2 snRNAs but eliminated U6 snRNA association with the U2 snRNP. Transcriptional inhibition reduced the formation of U4/U6 and U4/U6•U5 snRNPs, as shown by the decrease of U4 and U6 snRNAs levels in hPrp4 (asterisks) and hPrp8 precipitates. NC, negative control. (F) Schematic representation of snRNP interaction times with pre-mRNA. We assume that the U4/U6 proteins hPrp4 and hPrp31 leave with the U4 snRNA, whereas U6 snRNA stays associated with the activated spliceosome.

of immobile molecules in the splicing factor compartments. These results suggest the presence of snRNP-binding sites that are not dependent on transcription. In addition, after DRB treatment, snRNPs diffused slower in the splicing factor compartments than in the nucleoplasm, which correlated with FCS results. These data suggested an additional transient interaction not related to transcription and splicing that snRNPs encounter in the splicing factor compartments (Fig. S3 and Table II).

### U4/U6 and U4/U6•U5 snRNP integrity depends on active transcription

To characterize the molecular composition of snRNP complexes after transcriptional inhibition, we immunoprecipitated snRNP-specific proteins from DRB- or α-amanitin–treated cells (Fig. 3 E). Transcriptional inhibition had no effect on U1 and U2 snRNP integrity. However, we noticed that the small amount of U6 snRNAs that repeatedly copurified with U2 complexes in nontreated cells was lost after transcriptional inhibition. In addition, after transcriptional inhibition, the levels of coprecipitated U4 and U6 snRNAs with hPrp4 and hPrp8 proteins were reduced, illustrating that di- and tri-snRNP formation was impaired by this treatment.

### snRNPs interact independently with pre-mRNA

To characterize the interaction of snRNPs with pre-mRNA in living cells, we analyzed nontreated cells by FRAP (Fig. 3, B–D). To apply a proper model for data fitting, we performed FRAP experiments with half of the nucleus bleached and analyzed fluorescence recovery at various distances from the bleached

Published October 4, 2010

Table II. **Calculated parameters derived from FRAP measurements in BAC HeLa and E3 U2-OS cell lines**

| Proteins | Nucleoplasm | | | | Splicing factor compartments | | E3 gene loci |
|---|---|---|---|---|---|---|---|
| | $D_{f\ DRB}$ | $k_{off\ nt}$ | $k_{off\ isog}$ | $D_{f\ isog}$ | $D_{f\ DRB}$ | $k_{ofwnt}$ | $k_{off\ E3\ gene\ loci}$ |
| | $\mu m^2 s^{-1}$ | $s^{-1}$ | $s^{-1}$ | $\mu m^2 s^{-1}$ | $\mu m^2 s^{-1}$ | $s^{-1}$ | $s^{-1}$ |
| U1-70K[a,b] | 0.27 ± 0.02 | 1.57 ± 0.21 | 0.058 ± 0.007 | NA | 0.33 ± 0.05 | 1.07 ± 0.26 | NA |
| U2A′[a,b] | 0.56 ± 0.05 | 0.062 ± 0.005 | 0.047 ± 0.006 | NA | 0.17 ± 0.02 | 0.050 ± 0.08 | NA |
| hPrp31[a,b] | 0.55 ± 0.03 | 1.36 ± 0.30 | 0.63 ± 0.26 | NA | 0.24 ± 0.03 | 0.055 ± 0.005 | NA |
| hPrp4[a,b] | 0.47 ± 0.08 | 1.55 ± 0.13 | 0.90 ± 0.23 | NA | 0.32 ± 0.04 | 0.048 ± 0.007 | NA |
| hPrp8[a,b] | 0.27 ± 0.02 | 0.037 ± 0.004 | NA | 0.40 ± 0.02 | 0.10 ± 0.04 | 0.035 ± 0.005 | NA |
| Snu114[a,b] | 0.26 ± 0.03 | 0.032 ± 0.006 | NA | 0.27 ± 0.03 | 0.19 ± 0.02 | 0.038 ± 0.007 | NA |
| U1-70K[a,c] | 0.50 ± 0.05 | 1.88 ± 0.15 | ND | ND | ND | ND | 0.112 ± 0.010 |
| U2B″[c] | 0.61 ± 0.07 | 0.064 ± 0.005 | ND | ND | ND | ND | 0.056 ± 0.009 |
| hPrp4[c] | 0.75 ± 0.08 | 1.51 ± 0.20 | ND | ND | ND | ND | 0.043 ± 0.006 |
| hPrp8[a,c] | 0.37 ± 0.03 | 0.040 ± 0.003 | ND | ND | ND | ND | 0.030 ± 0.002 |

NA, not applicable. Diffusion coefficients $D_{f\ FRAP\ DRB}$ were calculated from fits of the FRAP curves measured in the nucleoplasm and the splicing factor compartments in DRB-treated cells. Dissociation rates $k_{off\ nt}$ were derived from fits of the FRAP curves measured in the nucleoplasm and splicing factor compartments of nontreated cells. Kinetic parameters $k_{off\ nucl\ isog}$ and $D_{f\ nucl\ isog}$ were derived from fits of the FRAP curves measured in the nucleoplasm of isoginkgetin-treated cells. Dissociation rates $k_{off\ E3\ gene\ loci}$ were calculated from fits of the FRAP curves measured at the transcription site of the E3 transgene in doxycycline-treated E3 U2-OS cells. The mean ± SEM is shown.

[a]BAC stable cell line.

[b]HeLa cells.

[c]E3 U2-OS cells.

area (Fig. S4). Distinct recovery profiles at different spots indicated that diffusion significantly contributed to fluorescence recovery and could not be omitted. Thus, FRAP curves were fitted with the full model comprising both diffusion and binding parameters (Eq. 3; Sprague et al., 2004; McNally, 2008). To reduce the number of fitted parameters, we used diffusion coefficients measured by FCS and fitted only parameters that described the binding event, association ($k^*_{on}$) and dissociation ($k_{off}$) rates. Additionally, by fitting the FRAP data with the diffusion coefficients measured after DRB treatment, similar $k_{off}$ values were calculated (unpublished data). Because $k^*_{on}$ also depends on the concentration of binding sites, which could not be easily determined, only $k_{off}$ values were used to describe the interaction between snRNPs and pre-mRNA.

$k_{off}$ values calculated for the U1 snRNP and the U4/U6 snRNP were >10-fold higher than $k_{off}$ for the U2 and U5 snRNPs, suggesting that U1 and U4/U6 snRNPs interact with pre-mRNA for a lesser time than U2 and U5 snRNPs (Table II). A schematic representation of snRNP interactions with pre-mRNA is shown in Fig. 3 F, in which the interaction time was calculated as an inversion of $k_{off}$. The longer association of U2 and U5 snRNPs with pre-mRNA likely reflects the stable interaction of these two snRNPs with pre-mRNA during splicing and is indicative of the in vivo splicing rate. Importantly, similar dissociation rates were obtained for different proteins from the same snRNP complex (hPrp8 and Snu114 from the U5 snRNP; hPrp4 and hPrp31 from the U4/U6 snRNP), which suggests that these values accurately reflect the behavior of snRNP complexes (Table II). In addition, FRAP curves of U1-70KΔ1–197–GFP protein did not indicate any stable interaction with pre-mRNA, and its fluorescence recovery was not affected by DRB treatment (Fig. S1 B). Conclusively, in untreated cells, FRAP measurements revealed that individual snRNPs have distinct dissociation rates, strongly indicating that snRNP interactions with pre-mRNA are independent.

To further show that $k_{off}$ values were indicative of snRNP binding to pre-mRNA, we performed FRAP measurements in cells treated with isoginkgetin, a potent splicing inhibitor. Isoginkgetin prevents U4/U6•U5 tri-snRNP recruitment to the spliceosome in vitro, resulting in the accumulation of prespliceosomal complex A that contains U1 and U2 snRNPs bound to pre-mRNA (Behzadnia et al., 2007; O'Brien et al., 2008). If $k_{off}$ represents the interaction of snRNPs with pre-mRNA, stabilization of complex A should decrease the $k_{off}$ value of the U1 snRNP. Splicing inhibition was confirmed by the enlargement of splicing factor compartments (Fig. 4 A; Kaida et al., 2007) and the accumulation of pre-mRNA from several genes (Fig. S5). Importantly, transcription was preserved, as measured by the incorporation of modified nucleotides (Fig. S2). Splicing inhibition resulted in the elevation of the U1 and U2 snRNP immobile fractions. Quantification of the mobile fraction revealed the dramatic decrease in the U1 snRNP $k_{off}$ value (Fig. 4, B and F; and Table II). The in vivo formation of a stable U1–U2–pre-mRNA complex was further confirmed by the coimmunoprecipitation of U1 snRNA with the U2A′ GFP-tagged protein from isoginkgetin-treated cells (Fig. 4 C). The prolonged residence time of the U1 snRNP on pre-mRNA complemented our measurements performed after transcriptional inhibition and demonstrated that the $k_{off}$ values signify snRNP interaction with pre-mRNA.

Splicing inhibition had a minor effect on the U4/U6 di-snRNP protein dissociation rate and only slightly increased the amount of U4/U6 di-snRNP immobile fraction, suggesting its transient interaction with stalled spliceosomal complexes (Fig. 4, D and F; and Table II). U5 snRNP FRAP curves measured in isoginkgetin-treated cells showed rapid recovery, and their quantification yielded diffusion coefficients that were comparable with the diffusion coefficients measured in DRB-treated cells (Fig. 4 E and Table II). Interestingly, we detected an apparent immobile fraction of U5 snRNP that might indicate either stalled spliceosomal complexes containing U5 snRNP or interactions occurring before the first step of splicing (Wyatt et al., 1992).

Published October 4, 2010

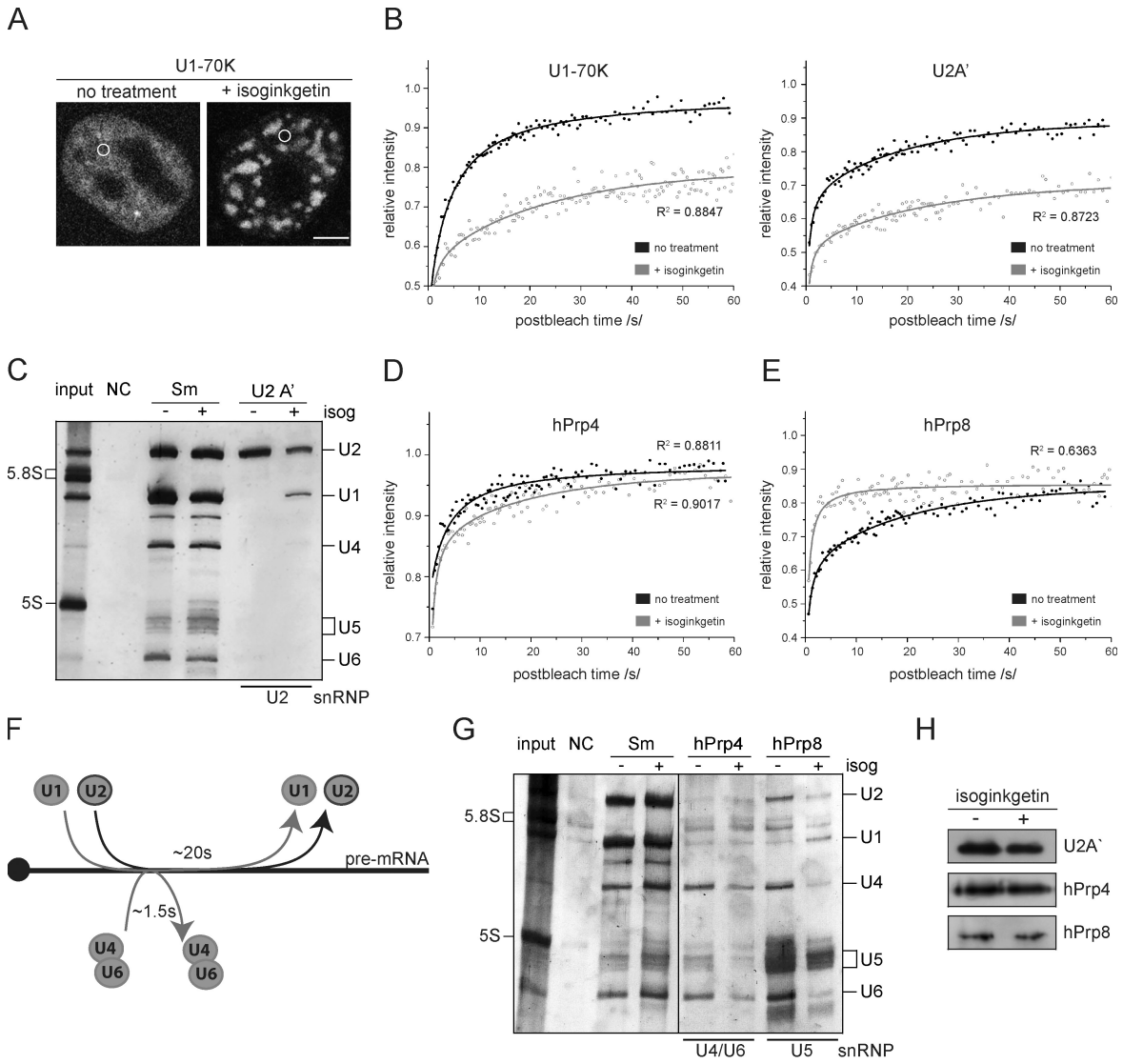


Figure 4. **The prolonged interaction of U1 and U2 snRNPs with pre-mRNA after splicing inhibition.** (A) After isoginkgetin treatment, GFP-tagged snRNP proteins relocalized to enlarged splicing factor compartments. FRAP measurements were performed in the nucleoplasm, as depicted by circles. Bar, 5 µm. (B) Splicing inhibition increased the immobile fractions and reduced the mobility of U1-70K and U2A′ (Table II). The mean of 10–12 measurements is shown. (C) Coimmunoprecipitation of U1 snRNA with U2A′-GFP after isoginkgetin (isog) treatment. (D) Splicing inhibition had minimal impact on U4/U6 snRNP mobility (Table II). (E) Splicing inhibition resulted in increased U5 snRNP mobility that can be described by a pure diffusion model. A portion of U5 snRNPs was bound in an immobile fraction. (F) Schematic representation of snRNP interaction times with pre-mRNA after splicing inhibition. (G) Coimmunoprecipitation of snRNAs from hPrp4-GFP and hPrp8-GFP cell lines with anti-GFP antibodies before and after isoginkgetin treatment. Splicing inhibition impairs U4/U6 di-snRNP and U4/U6•U5 tri-snRNP formation as shown by the reduced coprecipitation of U4 and U6 snRNAs with hPrp4 and hPrp8 proteins. The vertical black line indicates that intervening lanes have been spliced out. (H) The efficiency of GFP-tagged protein immunoprecipitation was verified by Western blot analysis. NC, negative control.

Collectively, our data showed that snRNP–pre-mRNA interactions can be measured by FRAP. In addition, the snRNPs that form the core active spliceosomal complex exhibited significantly longer interaction times (15–30 s), whereas U1 and U4/U6 snRNP proteins only transiently associated with pre-mRNA. This result is consistent with their role during intron definition (U1 snRNP) and spliceosome formation (U4/U6 snRNP).

### Splicing inhibition disrupts snRNP complexes

The different dynamic behavior of U4/U6 and U5 snRNP proteins in the presence of isoginkgetin implies impaired tri-snRNP formation. To analyze the integrity of tri-snRNP complexes after splicing inhibition, U4/U6 snRNP– and U5 snRNP–specific proteins were immunoprecipitated from isoginkgetin-treated cells, and coprecipitated snRNAs were analyzed (Fig. 4 G). After splicing inhibition, we detected a decrease in the level of U4 and U6 snRNAs associated with hPrp4 and hPrp8 proteins, confirming that di- and tri-snRNP formation is reduced. Interestingly, we noticed an increase in the association of U1 snRNA with U5 snRNP, possibly reflecting the observed immobilized fraction of U5 snRNP in FRAP measurements after splicing inhibition. Collectively, the immunoprecipitation data demonstrated that active splicing is necessary for di- and tri-snRNP integrity.

Published October 4, 2010

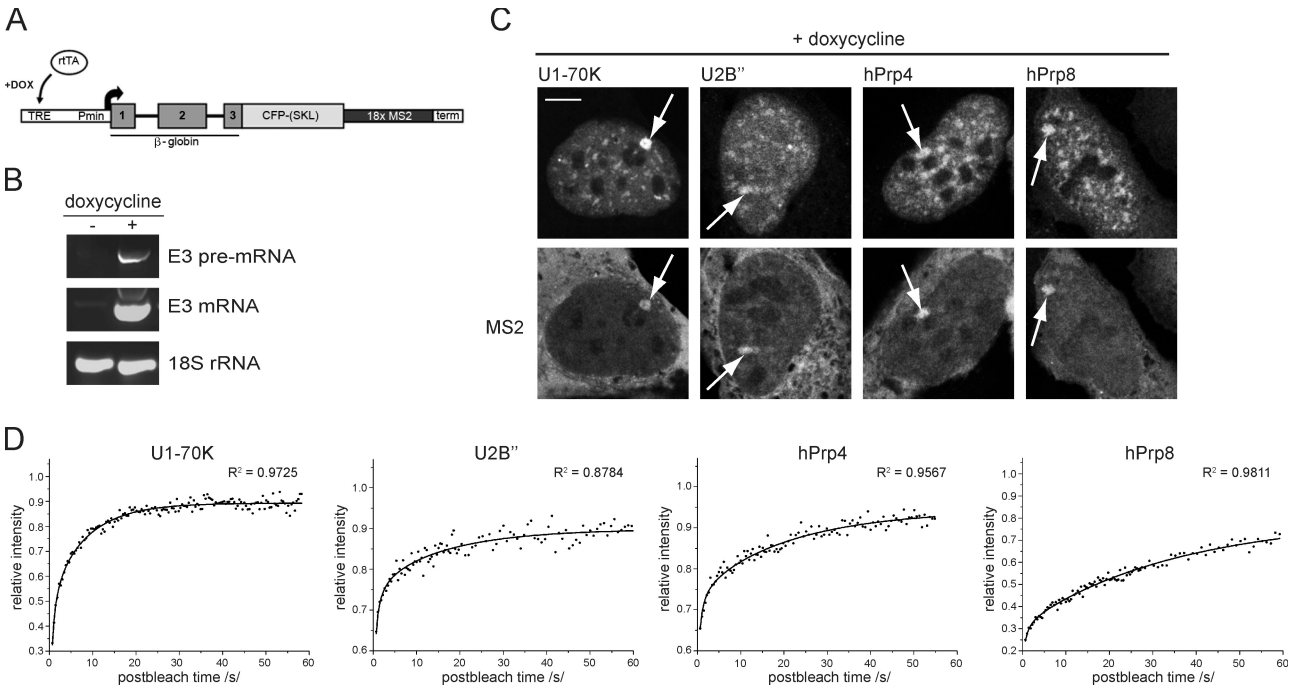


Figure 5. **snRNP interaction with E3 pre-mRNA.** (A) Schematic representation of the E3 gene stably integrated into the genome of the U2-OS Tet-On cell line. Expression of the E3 transgene is driven by a minimal cytomegalovirus promoter (Pmin) under the control of the tetracycline response element (TRE) and is induced by the presence of doxycycline (DOX) by the reverse transactivator, rtTA. The transgene transcript contains 18× MS2-binding sites, and the encoded protein (human β-globin) is fused to CFP-SKL. (B) E3 transgene expression before and after induction. (C) Doxycycline-treated E3 cells expressing different GFP-tagged snRNP proteins (top) and MS2-mRED protein (bottom). Note the localization of snRNP proteins at the site of active transgene transcription, as depicted by MS2-mRED accumulation (arrows). Bar, 5 µm. (D) FRAP analysis of snRNP dynamics at the active transcription site of the E3 transgene (Table II). A mean of 10–12 measurements is shown.

### Differential interaction of snRNPs with E3 pre-mRNA

Our results reveal the dynamics of snRNPs in the nucleoplasm and are a mean representation of snRNP behavior over numerous gene loci. To analyze snRNP dynamics at a specific gene locus, we used the inducible E3 U2-OS Tet-On cell system (Fig. 5 A; Shav-Tal et al., 2004; Darzacq et al., 2006) that either stably expressed from BACs GFP-tagged U1-70K (U1 snRNP) or hPrp8 (U5 snRNP) or transiently expressed GFP-tagged U2B″ (U2 snRNP) or hPrp4 (U4/U6 snRNP). Initially, we determined by FRAP that the diffusion coefficients and binding constants of individual snRNPs in the nucleoplasm of U2-OS cells are similar to that of HeLa cells (Table II). Doxycycline treatment of U2-OS cells resulted in the expression of E3 gene (Fig. 5 B), as visualized in situ via its interaction with the MS2-mRED protein (Fig. 5 C). After induction with doxycycline, snRNP-specific proteins localized to the site of active transgene transcription (Fig. 5 C). For quantification of snRNP interaction in the E3 gene loci, we used the radial binding model accounting for boundary effects in the cluster of binding sites (Eq. 4; Sprague et al., 2006). FRAP measurements performed at the site of transgene transcription revealed a surprising reduction in $k_{off}$ values. The greatest reductions detected were U1 snRNP (~17 fold) and U4/U6 snRNP (~35 fold). $k_{off}$ values for U2 snRNP and U5 snRNP dropped only partially (Fig. 5 D and Table II). These data illustrate that the dynamics of snRNPs differ at a specific gene compared with the mean values measured in the nucleoplasm. This might reflect either massive E3 gene transcription or specific splicing kinetics for E3 pre-mRNA. However, similar to nucleoplasmic spots, the binding rates of snRNPs differed at the artificial gene locus, again indicating the independent interaction of spliceosomal snRNPs with E3 pre-mRNAs.

## Discussion

We have successfully measured the dynamics of snRNP complexes in the cell nucleus and calculated the parameters that describe their movement throughout the nucleoplasm and their interactions with pre-mRNA. By using two different techniques, FRAP and FCS, we show that the diffusion of U1, U2, U4/U6, and U5 snRNPs is comparable and that their diffusion rates range between 0.2 and 0.8 $\mu m^2 s^{-1}$. Importantly, similar values were determined from both techniques and in two different cell lines. Our data are consistent with the diffusion rate of U1-70K in plants ($D_f$ = 0.7 $\mu m^2 s^{-1}$; Ali et al., 2008) and humans ($D_f$ = 0.5 $\mu m^2 s^{-1}$; (Grünwald et al., 2006) and the common snRNP protein, SmE, in human cells ($D_f$ = 0.8 $\mu m^2 s^{-1}$; Rino et al., 2007). snRNP movement is slower than the movement of non-snRNP splicing factors U2AF35/65, SF1, or SC35 ($D_f$ = 1.19–1.40 $\mu m^2 s^{-1}$; Rino et al., 2007). As diffusion efficiency of nuclear factors is largely determined by transient interactions (Phair and Misteli, 2001), these data indicate that snRNPs encounter extensive interactions within the nuclear environment.

Surprisingly, in all cases, we observed a pool of proteins that were apparently not incorporated into snRNP complexes and diffused rapidly throughout the nucleoplasm. Similarly, two fractions were identified for U1 snRNP, a slower fraction with

Published October 4, 2010

$D_f = 0.5\ \mu m^2 s^{-1}$ and a faster one with $D_f = 8.2\ \mu m^2 s^{-1}$ (Grünwald et al., 2006). In the case of the exon junction complex, free proteins were also detected (Schmidt et al., 2009). Together, these observations suggest that a fraction of unbound proteins is a common feature of proteins associated with multicomponent complexes.

The mathematical model used for FRAP data analysis not only enabled the estimation of diffusion rates but also allowed the approximation of snRNP-binding properties to nuclear components. Treatment of cells with transcriptional and splicing inhibitors demonstrated that in the nucleoplasm, the dominant interaction partner of snRNPs is pre-mRNA. U1 and U4/U6 snRNP components exhibit fast dynamic exchange with a residence time of <1 s, whereas U2 and U5 snRNP proteins interact longer with pre-mRNA with a residence time of ∼15–30 s (Fig. 3 F). If the spliceosome interacts with pre-mRNA in a big complex that contains all five snRNPs, individual snRNPs should have a similar residence time. Therefore, our results are consistent with the step-wise assembly model that proposes the transient interaction of U1 and U4/U6 snRNP proteins with pre-mRNA during the spliceosome formation and the longer association of U2 and U5 snRNP proteins that constitute the activated spliceosome (for reviews see Rino and Carmo-Fonseca, 2009; Wahl et al., 2009).

The residence times of the core splicing components (U2 and U5 snRNPs) can provide us with an estimate of the mean splicing rate in living cells. Our results suggest that splicing is accomplished within 30 s. Compared with previous studies that inferred that the splicing rate from intron removal after transcription induction or repression is between 0.5 and 10 min, our value is much faster (Audibert et al., 2002; Singh and Padgett, 2009). However, the rate of intron removal depends on many factors, including the rate of RNA synthesis and the rate of splice site recognition. Our results provide the first in vivo splicing rate estimate in a mammalian system that is independent of the speed of RNA synthesis and involves only the rate of splicing and assembly/disassembly of the spliceosome. We cannot absolutely rule out the possibility that GFP influences incorporation and behavior of tagged proteins in the spliceosome. However, GFP-tagged proteins are properly incorporated into snRNPs, GFP-Snu114 is able to partially rescue the proliferation phenotype, and two different proteins from the same snRNP complex exhibit identical kinetics. In addition, our results correlate well with the analysis of Miller spreads from *Drosophila melanogaster* embryos and ChIP data from yeast, which both suggest that splicing is accomplished within 1 min after spliceosome formation (Beyer and Osheim, 1988; Wetterberg et al., 2001; Görnemann et al., 2005). The immobile fractions of U2 and U5 snRNPs (∼10%) indicate that the splicing of some genes can take significantly longer than 30 s and might reflect delayed or regulated posttranscriptional splicing (LeMaire and Thummel, 1990; Wetterberg et al., 1996). Interestingly, the interaction of snRNPs with β-globin–based E3 pre-mRNA differs from the mean nucleoplasmic values. It was reported previously that the splicing rates of different introns vary significantly (Audibert et al., 2002). Therefore, it is plausible that the interaction of individual snRNPs and spliceosome assembly at one or both β-globin introns diverge from the mean. In addition, the accumulation of snRNPs at the artificial gene loci indicates a high rate of pre-mRNA production. Thus, snRNPs could be reused at this site and be involved in several splicing reactions without leaving the transcription loci, resulting in the observation of a prolonged residence time.

Our comprehensive analysis of snRNP dynamics in the cell nucleus reveals that snRNPs roam throughout the cell nucleus and continuously scan their environment via numerous transient interactions. Once snRNPs encounter a pre-mRNA substrate, they assemble the active splicing complex, accomplish the splicing reaction, and dissociate to be recycled for another round of splicing. Similar to other active multicomponent complexes (e.g., translation or transcription initiation complexes), the active spliceosome is formed from preassembled snRNPs only at the time and place of its need, allowing the assembly process to be regulated.

## Materials and methods

### Protein cloning and tagging

EST clones of human U1-70K and U2B″ were obtained from imaGenes. ORFs were amplified by the Expand long template PCR system and cloned into pEGFP-N1 (Takara Bio Inc.) using BamHI and EcoRI or BglI and EcoRI restriction sites. The truncated mutant U1-70KΔ1–197 protein was generated by deleting (using KpnI and BamHI restriction sites) the first 1–197 aa from the full-length human U1-70K cDNA and cloned into pEGFP-C1 (Takara Bio Inc.). The construct hPrp4 GFP-C2 was obtained from D.S. Horowitz (Cold Spring Harbor Laboratory, Cold Spring Harbor, NY). The construct MS2-mRED was generated upon subcloning the MS2 sequence from pMS2-EYFP-N1 (Huranová et al., 2009b) into pDsRed-Monomer-N1 (Takara Bio Inc.) using the XhoI and BamHI restriction sites.

### BAC tagging

BACs harboring the genes encoding human spliceosomal proteins (U1-70K, U2A′, hPrp4, hPrp31, and hPrp8) and the mouse homologue of the spliceosomal protein (Snu114) were obtained from the BACPAC Resources Center. The EGFP-IRES-Neo cassette (LAP) was inserted into the BAC by recombination as described previously (Zhang et al., 1998; Poser et al., 2008). In brief, the C-terminal tagging cassette (LAP) was PCR amplified with gene-specific primers carrying 50 nt of homology to the targeting sequence. Next, purified PCR product was inserted at the C terminus of the gene of interest using homologous recombination. Correct insertion of the tag was verified by PCR.

### Cell cultures and treatments

HeLa cells were cultured in high-glucose DME supplemented with 10% fetal calf serum, penicillin, and streptomycin (Invitrogen). Stable cell lines expressing the recombinant BACs were generated by transfection of HeLa cells with Effectene and selected with geneticin. The E3 U2-OS Tet-On cell line was generated by cointegrating the E3 gene (Shav-Tal et al., 2004) lacO repeats and puromycin resistance in U2-OS Tet-On cells. BAC E3 U2-OS cell lines were generated by transfection of E3 U2-OS cell lines with BACs and selecting with hygromycin. E3 cells were cultured in low-glucose DME containing 10% fetal calf serum, penicillin, and streptomycin. Transcription of the transgene in E3 U2-OS cells was induced using 6 µg/ml doxycycline. Doxycycline was added 6–10 h after transfection, and cells were assayed 12–16 h later. For transcriptional inhibition, cells were treated with 50 µM DRB (Sigma-Aldrich) or 50 µM α-amanitin (Sigma-Aldrich) for 5 h. For splicing inhibition, cells were treated overnight with 100 µM isoginkgetin (LGC Standards).

### Plasmids and siRNA transfection

Transient transfections of HeLa and E3 U2-OS cell lines with plasmids were performed using Fugene HD (Roche) according to the manufacturer's protocol. Preannealed siRNA duplexes were obtained from Applied Biosystems: hSnu114 3′ untranslated region, 5′-GCUGCUGUUGCCAUCUUGATT-3′. The negative control 1 siRNA from Applied Biosystems was used as a negative control. siRNA transfections were performed using Oligofectamine (Invitrogen) according to manufacturer's protocol. Cells were incubated for 48–72 h before further analysis.

### Proliferation assay after siRNA transfection

Cells were stained with 1 µM far-red fluorescent tracer DDAO-SE (Invitrogen) for 15 min at room temperature, plated, and, 24 h later, transfected with the appropriate siRNA. DDAO-SE intensity was measured at the time

Published October 4, 2010

of transfection and 50 h after transfection. Unstained cells were measured as a negative control. Dilution of DDAO-SE signal caused by an increasing number of cells was measured using a flow cytometer (633-nm laser; LSRII; BD) and analyzed with FlowJo software (Tree Star, Inc.).

**Antibodies**

Goat α-GFP polyclonal antibodies (raised against bacterially expressed full-length EGFP) used for immunoprecipitation were a gift from D. Drechsel (Max Planck Institute for Molecular Cell Biology and Genetics, Dresden, Germany). The Y12 antibody was produced in the Institute of Molecular Genetics (Academy of Sciences of the Czech Republic, Prague, Czech Republic) antibody facility using a hybridoma cell line. The mouse monoclonal α-BrdU antibody was purchased from Sigma-Aldrich. The following antibodies were used for Western blot analysis: the rabbit polyclonal antibody α-hSnu114 (U5-116K; gift from R. Lührmann, Max Planck Institute for Biophysical Chemistry, Göttingen, Germany), the mouse monoclonal α-tubulin antibody (gift from P. Dráber, Institute of Molecular Genetics), the mouse monoclonal α-GFP antibody (Santa Cruz Biotechnology, Inc.), and goat anti–mouse and anti–rabbit antibodies conjugated with horseradish peroxidase (The Jackson Laboratory).

**snRNP immunoprecipitation and Western blot analysis**

HeLa and HeLa BAC cell lines were grown on a 15-cm Petri dish for 28 h. Cells were treated with the aforementioned drugs before harvesting. Immunoprecipitation was performed as described previously (Huranová et al., 2009a) using the mouse α-Sm antibody (Y12) or goat α-GFP antibodies. RNA was extracted using phenol/chloroform, resolved on a 7-M urea-denaturing polyacrylamide gel, and silver stained. Alternatively, after immunoprecipitation, a fraction of Sepharose beads was resuspended in SDS-PAGE sample buffer, and proteins were resolved on 8% polyacrylamide gel. The immunoprecipitated proteins were detected with the α-GFP mouse monoclonal antibody and secondary anti–mouse antibodies conjugated with peroxidase using SuperSignal West Pico (Thermo Fisher Scientific).

**RT-PCR and quantitative PCR**

Total RNA was isolated 24 h after treatment using TRIZOL reagent (Invitrogen). cDNA was synthesized using gene-specific reverse primers and reverse transcription SuperScript III (Invitrogen). Taq polymerase was used to amplify cDNA. Controls without RT reaction were performed to verify no residual DNA contamination. Quantitative PCR was performed as described previously (Listerman et al., 2006), and the ratio of pre-mRNA to mRNA was calculated according to $R_{isoginkgetin} = 2^{(Ctpre\text{-}mRNA - CtmRNA)}$, normalized to DMSO-treated cells ($R_n = R_{isoginkgetin}/R_{DMSO}$), and plotted.

The following primers were used for RT-PCR and quantitative PCR: *18S* forward, 5′-TTGTTGGTTTTCGGAACTGAG-3′; *18S* reverse, 5′-GCAAATGCTTCGGCTCTGGTC-3′; *HBB* exon 1 intron 1 forward, 5′-CCTGGGCAGGTTGGTATCAAG-3′; *HBB* intron 2 exon 3 reverse, 5′-GCCCAGGAGCTGTGGGAGGAA-3′; *HBB* exon 1 exon 2 forward, 5`-CCTGGGCAGGCTGCTGGTGGT-3′; *HBB* exon 2 exon 3 reverse, 5′-GCCCAGGAGCCTGAAGTTCTC-3′; *LDHA* intron 14 exon 15 forward, 5′-CCTTTCAACTCTCTTTTGGCAACC-3′; *LDHA* intron 14 exon 15 reverse, 5′-AATCTTATTCTGGGGGGTCTGTTC-3′; *LDHA* exon 3 exon 5 forward, 5′-AGAACACCAAAGATTGTCTCTGGC-3′; *LDHA* exon 3 exon 5 reverse, 5′-TTTCCCCCATTAGGTAACGG-3′; *CACNA1G* exon 13 intron 13 forward, 5′-CTTCGGCAACTACGTGCTCT-3′; *CACNA1G* exon 13 intron 13 reverse, 5′-AATTGGAAGTGGGACTGCTG-3′; *CACNA1G* exon 13 forward, 5′-CCAGGAGGACTGGAACAAAG-3′; *CACNA1G* exon 13 reverse, 5′-AGAGCACGTAGTTGCCGAAG-3′; *FN1* intron 14 exon 15 forward, 5′-AAAATGATGTTGGCGACGAG-3′; *FN1* intron 14 exon 15 reverse, 5′-CGTCTCTCCTGTCACGGTGT-3′; *FN1* exon 24 forward, 5′-GGAAGAAGTGGTCCATGCTG-3′; and *FN1* exon 24 reverse, 5′-GGGACACTTTCCTTGTCATCC-3′.

**Image acquisition and processing**

Images were acquired using a confocal microscope (SP5; Leica) equipped with an oil immersion objective (HCX Plan-Apochromat 63× NA 1.40-0.6 oil, Lbd Blue CS), with 512 × 512–pixel format at 400-Hz scan speed and 1.6 Airy pinhole in 16-bit resolution. Frame averaging 6× was used in Fig. 1 A. Line averaging was used in following figures: 4× in Fig. 2 and 8× in Fig. 5 C. Figs. 3 A and 4 A are the first frames of the FRAP experiments, acquired at 1,400-Hz scan speed with no line averaging. All images were adjusted for brightness and contrast, and the raw images of Figs. 1 A, 2 (A–C), 3 A, 4 A, and 5 C are available on the JCB DataViewer.

**FCS acquisition, data processing, and analysis**

Cells plated on glass-bottomed Petri dishes (MatTek) were imaged using an inverted epifluorescence scanning confocal microscope (MicroTime 200; PicoQuant) equipped with an environmental chamber controlling $CO_2$ level and temperature. The FCS system contained a pulsed diode laser (LDH-P-C-470; 470 nm; PicoQuant) providing 80-ps pulses at up to a 40-MHz repetition rate, a proper filter set (cleanup filter Z470/20, dichroic mirror z490rdc, and bandpass filter HQ515/50; Chroma Technology Corp.), a water immersion objective (60× NA 1.2; Olympus), 50-µm pinhole, and a single-photon avalanche diode detector. Data were acquired in TTTR mode using SymphoTime200 software (PicoQuant), and F(L)CS data analysis was performed using home-built routines (DevC++ [Bloodshed Software] and OriginPro80 [OriginLab Corporation]). First, standard fluorescence intensity images of the cells using low laser power (1 µW at the back aperture of the objective) were acquired to properly localize the nucleus in all three dimensions. Subsequently, a set of point measurements (120 s each) with optimized power (3.6 µW at the back aperture of the objective, compromise between brightness and minimal photobleaching) were performed at selected locations within the nucleoplasm and the splicing factor compartments. FCS analysis of each point measurement consisted of (a) filtering out uncorrelated noise contributions (detector after pulsing and dark noise; Humpolícková et al., 2008), (b) estimation of SD for each lag time by splitting the measurement into 10 pieces (Benda et al., 2003), and (c) weighted nonlinear least square fit (Levenberg-Marquardt routine) by a theoretical model. For fitting the autocorrelation curves, we applied the pure diffusion model with one or two components using the standard equation for free three-dimensional translational diffusion:

$$G(\tau) = 1 + \frac{\sum_{i=1}^{R} \alpha_i^2 \langle N_i \rangle g_{3di}(\tau)}{\left[\sum_{i=1}^{R} \alpha_i \langle N_i \rangle^2\right]}, \quad (1)$$

where

$$g_{3\,dim}(\tau) = \left(1 + \frac{\tau}{\tau_{Di}}\right)^{-1} \left(1 + \frac{\tau}{SP^2 \tau_{Di}}\right)^{-1/2},$$

$\alpha_i$ is the experimental brightness of i-th species, $G(\tau)$ is the autocorrelation function, $N$ stands for the number of particles in the effective volume $V_{eff}$, $SP$ is a structure parameter, a constant for the given experimental setup, defined as the ratio of long, and short axis of the ellipsoidal detection volume $SP = z_0/\omega_0$, $\tau_D$ is diffusion time. The size of the effective volume is $V_{eff} = \pi^{3/2}\omega_0^2 z_0$.

For fitting the autocorrelation curves of EGFP, we applied the one-component three-dimensional anomalous diffusion model:

$$G_{3DAnomalous}(\tau) = 1 + \frac{1}{N}\left(1 + \left(\frac{\tau}{\tau_D}\right)^{\alpha}\right)^{-1} \left(1 + \frac{1}{SP^2}\left(\frac{\tau}{\tau_D}\right)^{\alpha}\right)^{-1/2},$$

where $\alpha$ is the anomaly exponent ($\alpha = 1$ for normal diffusion, $\alpha < 1$ for subdiffusion [usually encountered in cells], and $\alpha > 1$ for superdiffusion).

**FRAP acquisition, data processing, and analysis**

Cells were plated on glass-bottomed Petri dishes and, after 20–24 h, were transfected with the appropriate DNA constructs. The cells were imaged 22–24 h after transfection and/or drug treatment by using the SP5 confocal microscope equipped with an oil immersion objective (HCX Plan-Apochromat 63× NA 1.40-0.6 oil, Lbd Blue CS) and an environmental chamber controlling $CO_2$ level and temperature. Data acquisition was performed using a 512 × 512–pixel format at a 1,400-Hz scan speed and 1.6 Airy pinhole in 16-bit resolution. Bleaching (0.37 s) was performed with a circular spot 1.5 µm in diameter using the 488-nm line of a 100-mW argon laser operating at 100% laser power. Fluorescent recovery was monitored at low laser intensity (5–10% of a 100-mW laser) at 0.37-s intervals at the beginning of the recovery and at 0.37–1-s intervals when reaching the plateau of recovery. 10–15 separate FRAP measurements were performed for each experiment. FRAP curves were double normalized to whole cell fluorescence loss during acquisition and background. Normalized FRAP curves were fitted either with the pure diffusion model or full model equations, and the quality of the fit is illustrated with the $R^2$ value shown in the figures.

To fit the FRAP curves with the pure diffusion model, we used the following equation derived from Sprague et al. (2004):

$$frap(t) = e^{-\frac{\tau D}{2t}}\left(I_0\left(\frac{\tau D}{2t}\right) + I_1\left(\frac{\tau D}{2t}\right)\right). \quad (2)$$

The full model Laplace transform solution was used according to Sprague et al. (2004):

$$\overline{frap(p)} = \left(\frac{1-C_{eq}}{p}\right)\left(1+\frac{k^*_{on}}{p+k_{off}}\right)\left(2K_1(qw)I_1(qw)\right). \quad (3)$$

The actual recovery model is obtained by numerical inversion of transformation (Eq. 3) using the MATLAB routine invlap.m (Sprague et al., 2004), which is used to fit experimental data. $D_f$ values from FCS measurements were applied as an input for full model FRAP fitting. Before every fitting, we searched both $k^*_{on}$ and $k_{off}$ by varying in 10-fold increments from $10^{-5}$ to $10^2$ to find a good guess of both $k^*_{on}$ and $k_{off}$. The weighted Levenberg-Marquardt algorithm was used to cut off points having a big dislocation from the expected course leading to more precise fits.

To include boundary conditions, we used radial binding model expressed by the equation

$$\overline{frap(p)} = \frac{1}{p} - \frac{F_{eq,1eff}}{p}\left(1-\frac{2A}{q_1R_0}I_1(q_1R_0)\right)\times\left(1+\frac{k^*_{2on}/\gamma_{1eff}}{p+k_{2off}}\right) - \frac{C_{2eq}}{p+k_{2off}}. \quad (4)$$

The radial binding model was used according to Sprague et al. (2004). It assumes that diffusion constants outside and inside of the cluster are the same, i.e., $D_{1eff}$. The diffusion constant measured by FCS was applied. Binding constants measured in the nucleoplasm (Table II) were used as outside $k^*_{on}$ and $k_{off}$ values, and the radius of the nucleus was set to 7 µm.

**Online supplemental material**

Fig. S1 shows interaction of U1-70KΔ1–197 mutant with snRNAs and its mobility in the cell nucleus measured by FRAP. Fig. S2 illustrates transcriptional activity of cells after DRB and isoginkgetin treatment. Fig. S3 demonstrates the mobility of snRNPs in the splicing factor compartments before and after transcription inhibition. Fig. S4 shows the mobility of hPrp8 at different distances from the bleach area to demonstrate proper use of full model for fitting the FRAP data. Fig. S5 illustrates the effect of isoginkgetin on splicing of three different genes. Online supplemental material is available at http://www.jcb.org/cgi/content/full/jcb.201004030/DC1.

We are grateful to David Drechsel, David S. Horowitz, Pavel Dráber, and Reinhard Lührmann for gifts of reagents. We thank Tony Hyman for help with BAC recombineering, Martin Zapotocky for help with FRAP analysis, Ondrej Stepanek for help with flow cytometry and comments on the manuscript, members of the Staněk laboratory for comments on the manuscript, and Alicia Corlett for proofreading.

This work was supported by grants from the Max Planck Society (the Partner group program), the Czech Science Foundation (204/07/0133 and P305/10/0424), and the Academy of Sciences of the Czech Republic (KAN200520801 and AV0Z50520514) to D. Staněk, a grant from the Ministry of Education, Youth, and Sports of the Czech Republic (LC06063) to M. Hof, and a gift grant from the German Israeli Foundation (929-192.13/2006) to Y. Shav-Tal and K.M. Neugebauer. Y. Shav-Tal is the Jane Stern Lebell Family Fellow in Life Sciences at Bar-Ilan University.

Submitted: 6 April 2010
Accepted: 7 September 2010

## References

Ali, G.S., K.V. Prasad, M. Hanumappa, and A.S. Reddy. 2008. Analyses of in vivo interaction and mobility of two spliceosomal proteins using FRAP and BiFC. *PLoS One*. 3:e1953. doi:10.1371/journal.pone.0001953

Audibert, A., D. Weil, and F. Dautry. 2002. In vivo kinetics of mRNA splicing and transport in mammalian cells. *Mol. Cell. Biol.* 22:6706–6718. doi:10.1128/MCB.22.19.6706-6718.2002

Azubel, M., N. Habib, R. Sperling, and J. Sperling. 2006. Native spliceosomes assemble with pre-mRNA to form supraspliceosomes. *J. Mol. Biol.* 356:955–966. doi:10.1016/j.jmb.2005.11.078

Behzadnia, N., K. Hartmuth, C.L. Will, and R. Lührmann. 2006. Functional spliceosomal A complexes can be assembled in vitro in the absence of a penta-snRNP. *RNA*. 12:1738–1746. doi:10.1261/rna.120606

Behzadnia, N., M.M. Golas, K. Hartmuth, B. Sander, B. Kastner, J. Deckert, P. Dube, C.L. Will, H. Urlaub, H. Stark, and R. Lührmann. 2007. Composition and three-dimensional EM structure of double affinity-purified, human prespliceosomal A complexes. *EMBO J.* 26:1737–1748. doi:10.1038/sj.emboj.7601631

Benda, A., M. Beneš, V. Marecek, A. Lhotský, W.T. Hermens, and M. Hof. 2003. How to determine diffusion coefficients in planar phospholipid systems by confocal fluorescence correlation spectroscopy. *Langmuir*. 19:4120–4126. doi:10.1021/la0270136

Beyer, A.L., and Y.N. Osheim. 1988. Splice site selection, rate of splicing, and alternative splicing on nascent transcripts. *Genes Dev.* 2:754–765. doi:10.1101/gad.2.6.754

Bindereif, A., and M.R. Green. 1987. An ordered pathway of snRNP binding during mammalian pre-mRNA splicing complex assembly. *EMBO J.* 6:2415–2424.

Brody, E., and J. Abelson. 1985. The "spliceosome": yeast pre-messenger RNA associates with a 40S complex in a splicing-dependent reaction. *Science*. 228:963–967. doi:10.1126/science.3890181

Cao, W., and M.A. Garcia-Blanco. 1998. A serine/arginine-rich domain in the human U1 70k protein is necessary and sufficient for ASF/SF2 binding. *J. Biol. Chem.* 273:20629–20635. doi:10.1074/jbc.273.32.20629

Chodosh, L.A., A. Fire, M. Samuels, and P.A. Sharp. 1989. 5,6-Dichloro-1-beta-D-ribofuranosylbenzimidazole inhibits transcription elongation by RNA polymerase II in vitro. *J. Biol. Chem.* 264:2250–2257.

Chusainow, J., P.M. Ajuh, L. Trinkle-Mulcahy, J.E. Sleeman, J. Ellenberg, and A.I. Lamond. 2005. FRET analyses of the U2AF complex localize the U2AF35/U2AF65 interaction in vivo and reveal a novel self-interaction of U2AF35. *RNA*. 11:1201–1214. doi:10.1261/rna.7277705

Darzacq, X., N. Kittur, S. Roy, Y. Shav-Tal, R.H. Singer, and U.T. Meier. 2006. Stepwise RNP assembly at the site of H/ACA RNA transcription in human cells. *J. Cell Biol.* 173:207–218. doi:10.1083/jcb.200601105

Darzacq, X., Y. Shav-Tal, V. de Turris, Y. Brody, S.M. Shenoy, R.D. Phair, and R.H. Singer. 2007. In vivo dynamics of RNA polymerase II transcription. *Nat. Struct. Mol. Biol.* 14:796–806. doi:10.1038/nsmb1280

Dundr, M., U. Hoffmann-Rohrer, Q. Hu, I. Grummt, L.I. Rothblum, R.D. Phair, and T. Misteli. 2002. A kinetic framework for a mammalian RNA polymerase in vivo. *Science*. 298:1623–1626. doi:10.1126/science.1076164

Ellis, J.D., D. Llères, M. Denegri, A.I. Lamond, and J.F. Cáceres. 2008. Spatial mapping of splicing factor complexes involved in exon and intron definition. *J. Cell Biol.* 181:921–934. doi:10.1083/jcb.200710051

Görnemann, J., K.M. Kotovic, K. Hujer, and K.M. Neugebauer. 2005. Cotranscriptional spliceosome assembly occurs in a stepwise fashion and requires the cap binding complex. *Mol. Cell*. 19:53–63. doi:10.1016/j.molcel.2005.05.007

Gorski, S.A., S.K. Snyder, S. John, I. Grummt, and T. Misteli. 2008. Modulation of RNA polymerase assembly dynamics in transcriptional regulation. *Mol. Cell*. 30:486–497. doi:10.1016/j.molcel.2008.04.021

Grünwald, D., B. Spottke, V. Buschmann, and U. Kubitscheck. 2006. Intranuclear binding kinetics and mobility of single native U1 snRNP particles in living cells. *Mol. Biol. Cell*. 17:5017–5027. doi:10.1091/mbc.E06-06-0559

Humpolícková, J., L. Beranová, M. Stěpánek, A. Benda, K. Procházka, and M. Hof. 2008. Fluorescence lifetime correlation spectroscopy reveals compaction mechanism of 10 and 49 kbp DNA and differences between polycation and cationic surfactant. *J. Phys. Chem. B*. 112:16823–16829. doi:10.1021/jp806358w

Huranová, M., J. Hnilicová, B. Fleischer, Z. Cvacková, and D. Stanek. 2009a. A mutation linked to retinitis pigmentosa in HPRP31 causes protein instability and impairs its interactions with spliceosomal snRNPs. *Hum. Mol. Genet.* 18:2014–2023. doi:10.1093/hmg/ddp125

Huranová, M., J.A. Jablonski, A. Benda, M. Hof, D. Stanek, and M. Caputi. 2009b. In vivo detection of RNA-binding protein interactions with cognate RNA sequences by fluorescence resonance energy transfer. *RNA*. 15:2063–2071. doi:10.1261/rna.1678209

Jurica, M.S., and M.J. Moore. 2003. Pre-mRNA splicing: awash in a sea of proteins. *Mol. Cell*. 12:5–14. doi:10.1016/S1097-2765(03)00270-3

Jurica, M.S., L.J. Licklider, S.R. Gygi, N. Grigorieff, and M.J. Moore. 2002. Purification and characterization of native spliceosomes suitable for three-dimensional structural analysis. *RNA*. 8:426–439. doi:10.1017/S1355838202021088

Kaida, D., H. Motoyoshi, E. Tashiro, T. Nojima, M. Hagiwara, K. Ishigami, H. Watanabe, T. Kitahara, T. Yoshida, H. Nakajima, et al. 2007. Spliceostatin A targets SF3b and inhibits both splicing and nuclear retention of pre-mRNA. *Nat. Chem. Biol.* 3:576–583. doi:10.1038/nchembio.2007.18

Kim, S.A., K.G. Heinze, and P. Schwille. 2007. Fluorescence correlation spectroscopy in living cells. *Nat. Methods*. 4:963–973. doi:10.1038/nmeth1104

Konarska, M.M., and P.A. Sharp. 1986. Electrophoretic separation of complexes involved in the splicing of precursors to mRNAs. *Cell*. 46:845–855. doi:10.1016/0092-8674(86)90066-8

Konarska, M.M., and P.A. Sharp. 1988. Association of U2, U4, U5, and U6 small nuclear ribonucleoproteins in a spliceosome-type complex in absence of precursor RNA. *Proc. Natl. Acad. Sci. USA*. 85:5459–5462. doi:10.1073/pnas.85.15.5459

Kotovic, K.M., D. Lockshon, L. Boric, and K.M. Neugebauer. 2003. Cotranscriptional recruitment of the U1 snRNP to intron-containing genes in yeast. *Mol. Cell. Biol.* 23:5768–5779. doi:10.1128/MCB.23.16.5768-5779.2003

Lacadie, S.A., and M. Rosbash. 2005. Cotranscriptional spliceosome assembly dynamics and the role of U1 snRNA:5'ss base pairing in yeast. *Mol. Cell*. 19:65–75. doi:10.1016/j.molcel.2005.05.006

Lamond, A.I., and D.L. Spector. 2003. Nuclear speckles: a model for nuclear organelles. *Nat. Rev. Mol. Cell Biol.* 4:605–612. doi:10.1038/nrm1172

LeMaire, M.F., and C.S. Thummel. 1990. Splicing precedes polyadenylation during *Drosophila* E74A transcription. *Mol. Cell. Biol.* 10:6059–6063.

Listerman, I., A.K. Sapra, and K.M. Neugebauer. 2006. Cotranscriptional coupling of splicing factor recruitment and precursor messenger RNA splicing in mammalian cells. *Nat. Struct. Mol. Biol.* 13:815–822. doi:10.1038/nsmb1135

McNally, J.G. 2008. Quantitative FRAP in analysis of molecular binding dynamics in vivo. *Methods Cell Biol.* 85:329–351. doi:10.1016/S0091-679X(08)85014-5

Nelissen, R.L., C.L. Will, W.J. van Venrooij, and R. Lührmann. 1994. The association of the U1-specific 70K and C proteins with U1 snRNPs is mediated in part by common U snRNP proteins. *EMBO J.* 13:4113–4125.

Neugebauer, K.M. 2002. On the importance of being co-transcriptional. *J. Cell Sci.* 115:3865–3871. doi:10.1242/jcs.00073

O'Brien, K., A.J. Matlin, A.M. Lowell, and M.J. Moore. 2008. The biflavonoid isoginkgetin is a general inhibitor of Pre-mRNA splicing. *J. Biol. Chem.* 283:33147–33154. doi:10.1074/jbc.M805556200

Phair, R.D., and T. Misteli. 2001. Kinetic modelling approaches to in vivo imaging. *Nat. Rev. Mol. Cell Biol.* 2:898–907. doi:10.1038/35103000

Poser, I., M. Sarov, J.R. Hutchins, J.K. Hériché, Y. Toyoda, A. Pozniakovsky, D. Weigl, A. Nitzsche, B. Hegemann, A.W. Bird, et al. 2008. BAC TransgeneOmics: a high-throughput method for exploration of protein function in mammals. *Nat. Methods*. 5:409–415. doi:10.1038/nmeth.1199

Reed, R. 2000. Mechanisms of fidelity in pre-mRNA splicing. *Curr. Opin. Cell Biol.* 12:340–345. doi:10.1016/S0955-0674(00)00097-1

Rino, J., and M. Carmo-Fonseca. 2009. The spliceosome: a self-organized macromolecular machine in the nucleus? *Trends Cell Biol.* 19:375–384. doi:10.1016/j.tcb.2009.05.004

Rino, J., T. Carvalho, J. Braga, J.M. Desterro, R. Lührmann, and M. Carmo-Fonseca. 2007. A stochastic view of spliceosome assembly and recycling in the nucleus. *PLOS Comput. Biol.* 3:2019–2031. doi:10.1371/journal.pcbi.0030201

Rino, J., J.M. Desterro, T.R. Pacheco, T.W. Gadella Jr., and M. Carmo-Fonseca. 2008. Splicing factors SF1 and U2AF associate in extraspliceosomal complexes. *Mol. Cell. Biol.* 28:3045–3057. doi:10.1128/MCB.02015-07

Sapra, A.K., M.L. Ankö, I. Grishina, M. Lorenz, M. Pabis, I. Poser, J. Rollins, E.M. Weiland, and K.M. Neugebauer. 2009. SR protein family members display diverse activities in the formation of nascent and mature mRNPs in vivo. *Mol. Cell*. 34:179–190. doi:10.1016/j.molcel.2009.02.031

Schmidt, U., K.B. Im, C. Benzing, S. Janjetovic, K. Rippe, P. Lichter, and M. Wachsmuth. 2009. Assembly and mobility of exon-exon junction complexes in living cells. *RNA*. 15:862–876. doi:10.1261/rna.1387009

Shav-Tal, Y., X. Darzacq, S.M. Shenoy, D. Fusco, S.M. Janicki, D.L. Spector, and R.H. Singer. 2004. Dynamics of single mRNPs in nuclei of living cells. *Science*. 304:1797–1800. doi:10.1126/science.1099754

Singh, J., and R.A. Padgett. 2009. Rates of in situ transcription and splicing in large human genes. *Nat. Struct. Mol. Biol.* 16:1128–1133. doi:10.1038/nsmb.1666

Sperling, J., M. Azubel, and R. Sperling. 2008. Structure and function of the Pre-mRNA splicing machine. *Structure*. 16:1605–1615. doi:10.1016/j.str.2008.08.011

Sprague, B.L., and J.G. McNally. 2005. FRAP analysis of binding: proper and fitting. *Trends Cell Biol.* 15:84–91. doi:10.1016/j.tcb.2004.12.001

Sprague, B.L., R.L. Pego, D.A. Stavreva, and J.G. McNally. 2004. Analysis of binding reactions by fluorescence recovery after photobleaching. *Biophys. J.* 86:3473–3495. doi:10.1529/biophysj.103.026765

Sprague, B.L., F. Müller, R.L. Pego, P.M. Bungay, D.A. Stavreva, and J.G. McNally. 2006. Analysis of binding at a single spatially localized cluster of binding sites by fluorescence recovery after photobleaching. *Biophys. J.* 91:1169–1191. doi:10.1529/biophysj.105.073676

Staley, J.P., and C. Guthrie. 1998. Mechanical devices of the spliceosome: motors, clocks, springs, and things. *Cell*. 92:315–326. doi:10.1016/S0092-8674(00)80925-3

Stevens, S.W., D.E. Ryan, H.Y. Ge, R.E. Moore, M.K. Young, T.D. Lee, and J. Abelson. 2002. Composition and functional characterization of the yeast spliceosomal penta-snRNP. *Mol. Cell*. 9:31–44. doi:10.1016/S1097-2765(02)00436-7

Tardiff, D.F., and M. Rosbash. 2006. Arrested yeast splicing complexes indicate stepwise snRNP recruitment during in vivo spliceosome assembly. *RNA*. 12:968–979. doi:10.1261/rna.50506

Tardiff, D.F., S.A. Lacadie, and M. Rosbash. 2006. A genome-wide analysis indicates that yeast pre-mRNA splicing is predominantly posttranscriptional. *Mol. Cell*. 24:917–929. doi:10.1016/j.molcel.2006.12.002

Urlaub, H., V.A. Raker, S. Kostka, and R. Lührmann. 2001. Sm protein-Sm site RNA interactions within the inner ring of the spliceosomal snRNP core structure. *EMBO J.* 20:187–196. doi:10.1093/emboj/20.1.187

Wahl, M.C., C.L. Will, and R. Lührmann. 2009. The spliceosome: design principles of a dynamic RNP machine. *Cell*. 136:701–718. doi:10.1016/j.cell.2009.02.009

Wassarman, D.A., and J.A. Steitz. 1992. Interactions of small nuclear RNA's with precursor messenger RNA during in vitro splicing. *Science*. 257:1918–1925. doi:10.1126/science.1411506

Wetterberg, I., G. Baurén, and L. Wieslander. 1996. The intranuclear site of excision of each intron in Balbiani ring 3 pre-mRNA is influenced by the time remaining to transcription termination and different excision efficiencies for the various introns. *RNA*. 2:641–651.

Wetterberg, I., J. Zhao, S. Masich, L. Wieslander, and U. Skoglund. 2001. In situ transcription and splicing in the Balbiani ring 3 gene. *EMBO J.* 20:2564–2574. doi:10.1093/emboj/20.10.2564

Will, C.L., and R. Lührmann. 2001. Spliceosomal UsnRNP biogenesis, structure and function. *Curr. Opin. Cell Biol.* 13:290–301. doi:10.1016/S0955-0674(00)00211-8

Wyatt, J.R., E.J. Sontheimer, and J.A. Steitz. 1992. Site-specific cross-linking of mammalian U5 snRNP to the 5′ splice site before the first step of pre-mRNA splicing. *Genes Dev.* 6:2542–2553. doi:10.1101/gad.6.12b.2542

Zhang, Y., F. Buchholz, J.P. Muyrers, and A.F. Stewart. 1998. A new logic for DNA engineering using recombination in *Escherichia coli*. *Nat. Genet.* 20:123–128. doi:10.1038/2417

Published October 4, 2010



Huranová et al., http://www.jcb.org/cgi/content/full/jcb.201004030/DC1

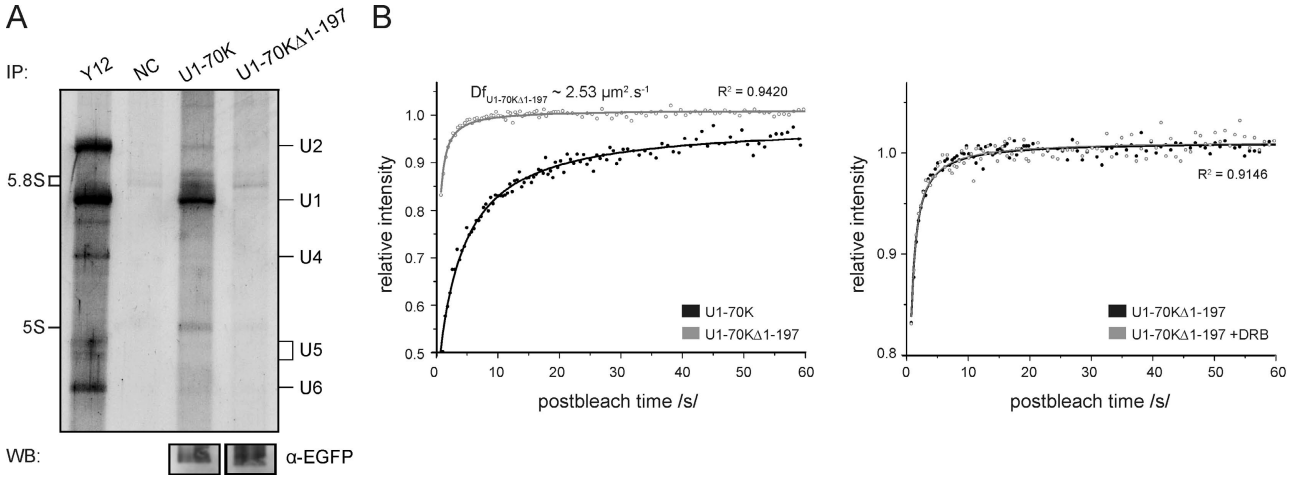


Figure S1. **Truncated protein U1-70KΔ1–197 is incorporated in U1 snRNP.** (A) Coimmunoprecipitation of U1 snRNA was performed from the U1-70K–GFP cell line or HeLa cells transiently expressing U1-70KΔ1–197–GFP using anti-GFP antibodies. The bottom panel shows the immunoprecipitation (IP) efficiency of the GFP-tagged U1-70K and U1-70KΔ1–197 proteins verified by Western blot (WB) analysis. NC, negative control. (B) FRAP analysis of U1-70KΔ1–197–GFP was performed in the nucleoplasm of untreated cells (left) or cells treated with the transcription inhibitor DRB (right). Both recovery curves were fitted well with the pure diffusion model. In contrast to the wild-type U1-70K, the truncated mutant exhibited fast recovery that was not affected by transcriptional inhibition, indicating no stable interactions with pre-mRNA.

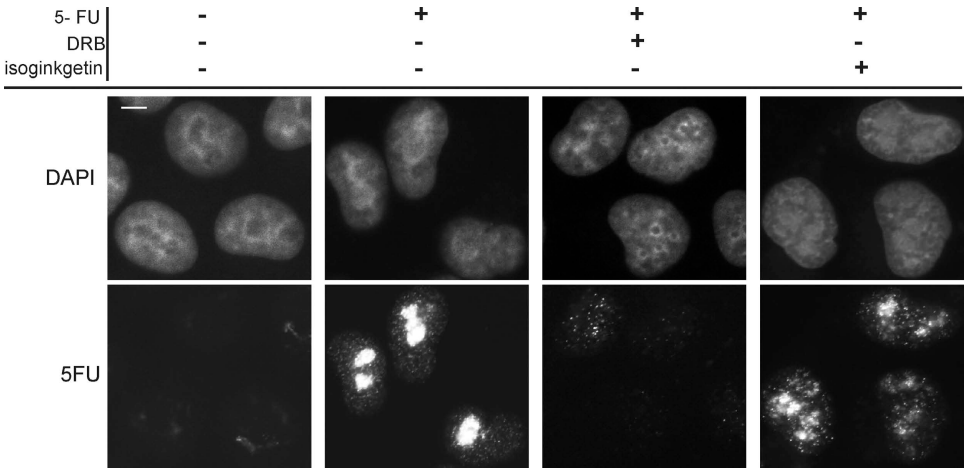


Figure S2. **DRB but not isoginkgetin inhibits transcription.** Cells were incubated with 5-fluorouridine (5-FU) that was incorporated into newly synthesized RNA. After 30 min of treatment, cells were fixed, and 5-fluorouridine–labeled RNA was detected by indirect immunofluorescence using antibromodeoxyuridine antibodies that cross-react with 5-fluorouridine. Transcription is inhibited by treatment with the RNA polymerase II inhibitor DRB but not by treatment with the splicing inhibitor isoginkgetin. Bar, 5 μm.

Published October 4, 2010

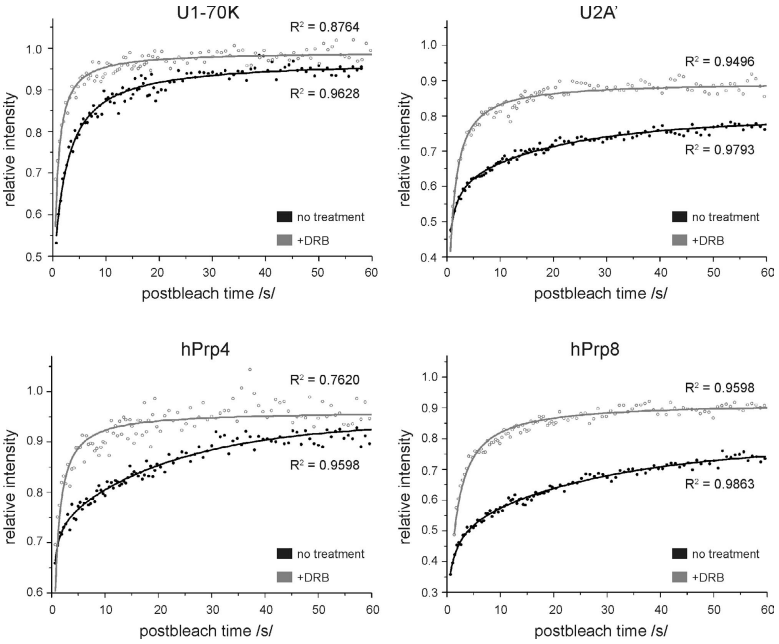


Figure S3. **FRAP measurements of snRNPs in the splicing factor compartments before and after transcriptional inhibition with DRB.** In nontreated cells, snRNPs exhibit slower movement compared with the nucleoplasm. Increased mobility of snRNPs after DRB treatment indicated interaction with pre-mRNA, and incomplete recovery pointed to additional binding sites for snRNPs in the splicing factor compartments. See also Table II.

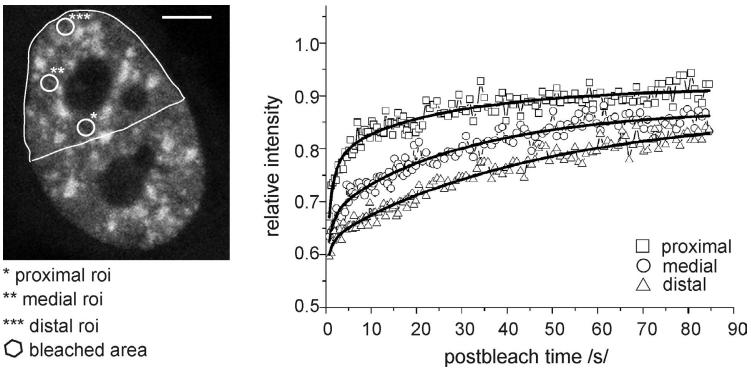


Figure S4. **The role of diffusion in FRAP recovery curves.** To determine the role of diffusion in the fluorescence recovery, a half of the nucleus of hPrp8-GFP cells was bleached and fluorescence recovery analyzed in three spots in the nucleoplasm with different distances from the bleached area (Phair et al., 2004; Beaudouin et al., 2006). hPrp8-GFP recovery profiles differed in these spots, indicating that the hPrp8 dynamic behavior is diffusion coupled. Bar, 5 µm.

Published October 4, 2010

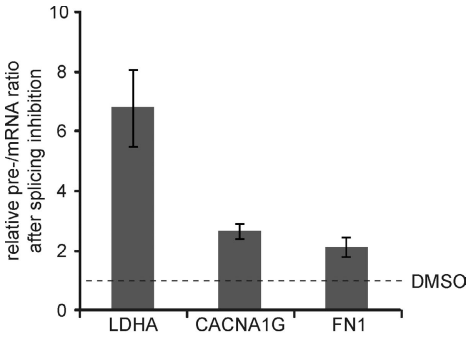


Figure S5. **Isoginkgetin inhibits pre-mRNA splicing of several genes.** Quantitative RT-PCR analysis of pre-mRNA and mRNA abundance was performed in control (DMSO)- and isoginkgetin-treated cells. The ratio of pre-mRNA after splicing inhibition was normalized to control cells, and the ratio was set to one (dashed line). The increased pre-mRNA ratio in isoginkgetin-treated cells demonstrates an elevated abundance of pre-mRNA.The mean and SD of two independent experiments are shown.

## References

Beaudouin, J., F. Mora-Bermúdez, T. Klee, N. Daigle, and J. Ellenberg. 2006. Dissecting the contribution of diffusion and interactions to the mobility of nuclear proteins. *Biophys. J.* 90:1878–1894. doi:10.1529/biophysj.105.071241

Phair, R.D., S.A. Gorski, and T. Misteli. 2004. Measurement of dynamic protein binding to chromatin in vivo, using photobleaching microscopy. *Methods Enzymol.* 375:393–414. doi:10.1016/S0076-6879(03)75025-3